Available online at www.sciencedirect.com
ScienceDirect
International Journal of Heat and Mass Transfer 50 (2007) 2557–2570
International Journal of HEAT and MASS TRANSFER
www.elsevier.com/locate/ijhmt

Dynamics of a vapor bubble on a heated substrate

S.W. Joo [a,*], M.S. Park [b]

[a] School of Mechanical Engineering, Yeungnam University, Gyongsan 712-749, Republic of Korea
[b] Department of Engineering, Science and Applied Mathematics, Northwestern University, Evanston, IL 60208, USA

Received 23 February 2006; received in revised form 20 November 2006
Available online 7 March 2007

Abstract

The dynamics of a vapor bubble between its liquid phase and a heated plate is studied in relation to the breakdown and recovery of the film boiling. By examining the expansion and the contraction of the vapor bubble the film boiling and transition boiling states are predicted. Conservation laws in the vapor, solid, and liquid phases are invoked along with fully nonlinear, coupled, free boundary conditions. These coupled system of equations are reduced to a single evolution equation for the local thickness of the vapor bubble by using a long-wave asymptotics, which is then solved numerically to yield the transient motion of the vapor bubble. Of the numerous parameters involved in this complex phenomenon we focus on the effects of the degree of superheat from the solid plate, that of the supercooling through the liquid, and the wetting/dewetting characteristics of the liquid on the solid plate. A material property of the substrate thus is incorporated into the criteria for the film boiling based on hydrodynamic models.

Keywords: Bubble; Film boiling; Evolution equation; Moving boundary; Contact line

1. Introduction

When a pool of liquid is heated from below beyond a critical temperature, a complex sequence of boiling phenomena occurs as the superheat is increased. The states are usually classified as natural convection, nucleate boiling, transition boiling, and film boiling in the order they appear as the heating intensity is increased, and have been studied intensively, as reviewed by Rohsenow [13] and Dhir [5] and in a monograph by Carey [3] among many others.

When the superheat is sufficient, the film-boiling state is reached, where the liquid is no longer in contact with the heated bottom, but is separated by a continuous film of the vapor. Film boiling has been relatively amenable to more straightforward studies, as discussed in the aforementioned reviews.

An important parameter used to characterize boiling is the superheat, the difference between the solid temperature and the saturation temperature. The saturation temperature is the liquid–vapor equilibrium temperature corresponding to the ambient saturation pressure. Another important parameter is the subcooling, the difference between the saturation temperature and the ambient liquid temperature far from the film. These two parameters are easily controlled in experiments and characterize the different regimes of pool boiling. For small superheat, liquid covers the entire heating surface, and vapor bubbles are only produced at isolated points on the surface. As the superheat is increased, patches of vapor cover portions of the heating surface while other portions are still wetted by the liquid in a process known as transition boiling. Coalescence of these vapor patches into a continuous film at a higher superheat gives rise to the onset of the film boiling. One of the more important tasks subject to further discussions in the study of boiling is an accurate assessment of the critical heat flux for the film boiling.

The experimental data of Witte and Lienhard [15] on the film boiling show that the onset of film boiling depends on the wetting characteristics of the liquid on the solid surface.

* Corresponding author. Tel.: +82 53 810 2568; fax: +82 53 810 4627.
E-mail address: swjoo@yumail.ac.kr (S.W. Joo).

0017-9310/$ - see front matter © 2007 Elsevier Ltd. All rights reserved.
doi:10.1016/j.ijheatmasstransfer.2006.11.044

Nomenclature

$a(t)$	contact line location
B	ratio of gravity to surface tension
d	initial thickness of bubble
D_ρ	ratio of vapor density to liquid density
D_μ	ratio of vapor viscosity to liquid viscosity
D_κ	ratio of vapor thermal diffusivity to liquid thermal diffusivity
E	evaporation number
g	gravitational acceleration
J	mass transfer through liquid–vapor interface
k	thermal conductivity
K	ratio of a typical evaporation rate for a film thickness to the absolute rate of evaporation at the saturated temperature
L	dimensionless **L**
L	latent heat
$\vec{n}$	normal vector
P	Prandtl number
R	Reynolds number for vapor
$\vec{t}$	tangential vector
t	time
T_L	liquid temperature
T_S	solid plate temperature
T_{SAT}	saturated temperature of liquid
T_{SUB}	subcooling temperature
T_{SUP}	superheated temperature
$V(u,w)$	velocity vector
x	horizontal coordination
z	vertical coordination
Z_L	distance from the solid plate to liquid far from the bubble
Z_S	solid plate thickness
$'$	dimensional parameters

Greek symbols

β	dimensionless wavenumber
Γ_κ	ratio of vapor thermal diffusivity to solid thermal diffusivity
θ	solid plate temperature
Θ	contact angle
ρ	vapor density
μ	vapor viscosity
ϵ	ratio of initial bubble thickness to its radius
h	film thickness

Superscript

$\hat{}$	liquid phase

Subscripts

L	liquid phase
S	solid phase

The minimum-heat-flux point is found to decrease as the advancing contact angle increases. This suggests that intermittent liquid–solid contact occurs even in film boiling. The increased heat transfer at the wetted portion of the heating surface may quickly evaporate the liquid and return the system to the film-boiling state, or the liquid may spread across the surface and bring the system into the transition-boiling regimes. The effect of the liquid–solid contact line is investigated in this study. Stability analysis ([12], for example) of the vapor–liquid interface in film boiling also shows a spontaneous incipient rupture process of the vapor film. The liquid, upon touching the bottom (vapor-film rupture), may either spread (toward transition boiling) or vaporize (toward film boiling), depending upon the competitive effects of evaporation and feeding from the liquid bulk above. The dynamics of the wetting/dewetting process, or the liquid/solid contact, near the onset of film boiling again is an important subject for investigation.

Anderson and Davis [1] formulated a new contact-line condition based on a mass balance across the evaporating interface, and he assumed that the relation between the macroscopic contact angle and the fluid velocity at the contact line is approximately given by its non-evaporative form. The lack of direct experimental observations of the fluid velocity at the contact line when evaporation is present hinders the use of an empirical relation that includes evaporative effects.

Fig. 1 illustrates a possible scenario for switching between the film and the transition boiling. The liquid above the vapor in a film boiling state may touch the heated substrate near the critical heat flux, generating a series of vapor bubbles separated by the liquid. If the heat flux from below is large enough, the vapor bubbles will expand

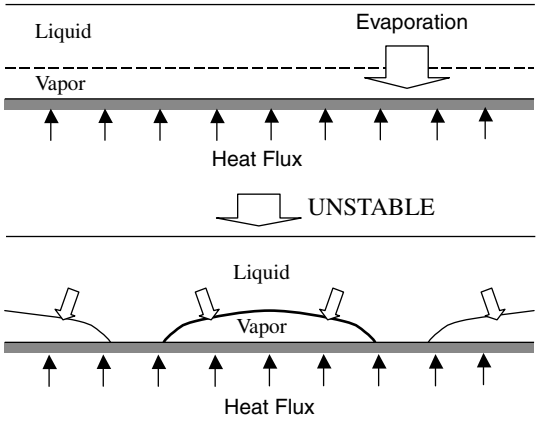

Fig. 1. Configuration for film boiling and transition boiling.

to coalesce with each other. The liquid will then be displaced back to be separated from the substrate; the film boiling state is recovered. Below a critical heat flux the evaporation from the liquid to vapor bubbles is insufficient to make them grow; the film boiling state is broken. In this study, we focus on one such bubble, and determine the conditions for its expansion and contraction. The criteria for the onset of film boiling thus is further revealed.

2. Formulation

2.1. Modeling a vapor bubble

A two-dimensional vapor bubble lies on a heated solid plate as shown in Fig. 2. The heated plate supplies heat flux to the liquid and the vapor. The vapor bubble is surrounded by the liquid and stays symmetric. The solid plate maintains a constant temperature T'_S, above the saturation temperature of the liquid T'_{SAT}. At a distance Z'_L above the solid plate the liquid temperature is controlled at T'_L, below the saturated temperature. The liquid–vapor interface is taken as $z' = h'(x', t')$, where h' is a single-valued function of horizontal position x' and time t'. The liquid and vapor are both treated as incompressible Newtonian fluids with constant material properties. The temperature of the solid is denoted by θ'. Since the liquid–vapor interface is a free surface, the film thickness h' is unknown a priori. J' is the mass flux across the liquid–vapor interface due to evaporation. Finally, Θ' is a contact angle against the solid plate and the edge of liquid–vapor interface. Normal vector and tangential vector at the liquid–vapor interface can be shown in the following equations.

$$\vec{n} = \frac{1}{\sqrt{1+h'^2_{x'}}}(h'_{x'}, -1), \quad \vec{t} = \frac{1}{\sqrt{1+h'^2_{x'}}}(1, h'_{x'}). \tag{1}$$

In Fig. 2 the direction toward the vapor is positive. Contact-line location at which the liquid–vapor interface meets solid plate is chosen by $x' = a'(t')$. Three phases, solid, liquid and vapor, are coupled dynamically, forming a multi-phase and free-boundary problem with moving vapor–liquid interface, which is a function of location x' and time t', and the moving contact line, a function of time t'. To solve the problem, we consider mass, momentum, and energy conservation for the liquid and vapor and energy conservation for the solid plate. Boundary conditions are rather involved in this complex problem, and are discussed below [6–11].

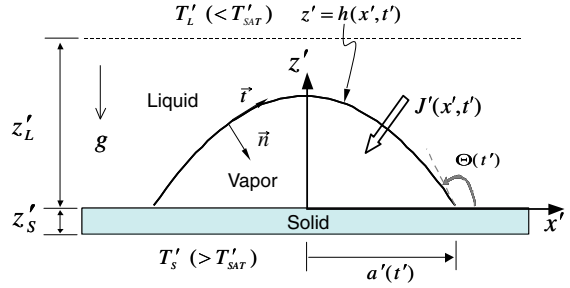

Fig. 2. Configuration for a vapor bubble on a heated solid.

2.2. Dimensionless governing equations

We scale the governing system using the initial thickness of the bubble d and the static pressure difference $\Delta\rho g d$, where g is the gravity acceleration, and $\Delta\rho = \rho_L - \rho$ is the difference between the liquid and the vapor density. A typical velocity scale $gd^2\Delta\rho/\mu$ is formed by balancing pressure and viscous forces in the vapor film, where μ is the vapor viscosity. The time scale $\mu/gd\Delta\rho$ is found by dividing the length scale by the velocity scale. The dimensionless temperature is obtained by subtracting the saturated temperature T'_{SAT} from the dimensional temperature and then dividing by the saturated temperature. For the evaporation flux, the energy balance at the interface is scaled by $k\Delta T'_{SUP}/d\mathbf{L}$, where $\Delta T'_{SUP} = T'_S - T'_{SAT}$, $\mathbf{L}$ is latent heat. Here the prime ($'$) denotes dimensional quantities. $V(u,w)$ is the velocity vector, where the hat ($\wedge$) is used for liquid phase. The temperature field in the solid phase is denoted by θ.

Dimensionless length scales are then written as

$$x = \frac{1}{d}x', \quad z = \frac{1}{d}z', \quad h = \frac{1}{d}h', \quad a = \frac{1}{d}a'. \tag{2}$$

Dimensionless time, mass flux, and contact angel are shown as, respectively,

$$t = \frac{gd\Delta\rho}{\mu}t', \quad J = \frac{d\mathbf{L}}{k\Delta T'_{SUP}}J', \quad \Theta = \Theta'. \tag{3}$$

Dimensionless velocity, temperature and pressure are

$$V = \frac{\mu}{gd^2\Delta\rho}V', \quad p = \frac{p' + \rho g z'}{\Delta\rho g d}, \quad T = \frac{T' - T'_{SAT}}{T'_{SAT}}, \tag{4}$$

for the vapor and

$$\hat{V} = \frac{\mu}{gd^2\Delta\rho}\hat{V}', \quad \hat{p} = \frac{\hat{p}\hat{V} + \rho_L g z'}{\Delta\rho g d}, \quad T = \frac{\hat{T}\hat{V} - T'_{SAT}}{T'_{SAT}}, \tag{5}$$

for the liquid. For the solid we have

$$\theta = \frac{\theta' - T'_{SAT}}{T'_{SAT}}. \tag{6}$$

With the above dimensionless variables, the continuity equations for vapor and liquid are written as

$$u_x + w_z = 0, \tag{7}$$

$$\hat{u}_x + \hat{w}_z = 0. \tag{8}$$

Horizontal and vertical components of the dimensionless momentum equation in the vapor phase are

$$R(u_t + uu_x + wu_z) = -p_x + u_{xx} + u_{zz} = 0, \tag{9}$$

$$R(w_t + uw_x + ww_z) = -p_z + w_{xx} + w_{zz} = 0, \tag{10}$$

where $R = \rho\Delta\rho g d^3/\mu^2$ is Reynolds number for vapor phase.

Horizontal and vertical components of the dimensionless momentum equation in the liquid phase are

$$RD_\rho^{-1}(\hat{u}_t + \hat{u}\hat{u}_x + \hat{w}\hat{u}_z) = -\hat{p}_x + D_\mu^{-1}(\hat{u}_{xx} + \hat{u}_{zz}) = 0, \quad (11)$$

$$RD_\rho^{-1}(\hat{w}_t + \hat{u}\hat{w}_x + \hat{w}\hat{w}_z) = -\hat{p}_z + D_\mu^{-1}(\hat{w}_{xx} + \hat{w}_{zz}) = 0, \quad (12)$$

where $D_\rho = \rho/\rho_L$ is the ratio of vapor density to liquid density, and $D_\mu = \mu/\mu_L$ is the ratio of the vapor to the liquid viscosity.

Dimensionless energy equations for vapor, liquid and solid are, respectively,

$$RP(T_t + uT_x + wT_z) = T_{xx} + T_{zz}, \quad (13)$$

$$RPD_\kappa(\widehat{T}_t + \hat{u}\widehat{T}_x + \hat{w}\widehat{T}_z) = \widehat{T}_{xx} + \widehat{T}_{zz}, \quad (14)$$

$$RP\Gamma_\kappa\theta_t = \theta_{xx} + \theta_{zz}, \quad (15)$$

where $P = \mu/\rho\kappa$ is Prandtl number, $D_\kappa = \kappa/\kappa_L$ is the ratio of the vapor to the liquid thermal diffusivity, and $\Gamma_\kappa = \kappa/\kappa_S$ is the ratio of the vapor to the solid thermal diffusivity.

2.3. Dimensionless boundary conditions

The temperature at the bottom side of the solid plate $z = -z_S$ is kept constant, so that

$$\theta = \Delta T_{SUP}, \quad (16)$$

where $\Delta T_{SUP} = \Delta T'_{SUP}/T'_{SAT}$ is the dimensionless superheat, and z_S is the dimensionless thickness of the solid plate.

At the solid–vapor interface $z = 0$, the Navier slip model, no-penetration condition, continuous temperature, and the continuous heat flux are taken as, respectively,

$$u = \frac{\beta}{h}u_z, \quad w = 0, \quad \theta = T, \quad \Gamma_k T_z = \theta_z, \quad (17)$$

where the slip coefficient is very small. Γ_k is the ratio of the heat conductivity for the solid to that for the liquid.

A constant temperature condition is imposed at $z = z_L$ to implement the subcooling, so that

$$\widehat{T} = -\Delta T_{SUB}, \quad (18)$$

where $T_{SUB} = \Delta T'_{SUB}/T'_{SAT}$ is the dimensionless subcooling.

At the liquid–vapor interface $z = h(x,t)$ dimensionless boundary conditions for mass conservation, energy conservation, the equilibrium of normal stress and shear stress, continuous tangential velocity, continuous temperature and mass flux are imposed, as explained by Delhaye [4], Burelbach and Bankoff [2], and Panzarella et al. [12].

The conservation of mass for the vapor and the liquid phase at the liquid–vapor interface are written as, respectively,

$$E\Delta T_{SUP}J = (h_t + uh_x - w)(1 + h_x^2)^{-1/2}, \quad (19)$$

$$E\Delta T_{SUP}D_\rho J = (h_t + \hat{u}h_x - \hat{w})(1 + h_x^2)^{-1/2}, \quad (20)$$

where the evaporation number $E = k\mu T'_{SAT}/\rho\Delta\rho\mathbf{L}gd^3$ is the ratio of viscosity to evaporative time.

The conservation of energy at the liquid–vapor interface is

$$\Delta T_{SUP}J + \frac{E^2\Delta T_{SUP}^3(1 - D_\rho^2)J^3}{2L} + \frac{T_z - T_x h_x - D_k^{-1}(\widehat{T}_z - \widehat{T}_x h_x)}{(1 + h_x^2)^{1/2}} + \frac{2\Delta T_{SUP}J}{LR(1 + h_x^2)}\left[h_x(u_z + w_x) - (h_x^2 - 1)u_x - \frac{D_\rho}{D_\mu}((\hat{u}_z + \hat{w}_x) - (h_x^2 - 1)\hat{u}_x)\right] = 0, \quad (21)$$

where $D_k = k/k_L$ is the ratio of the vapor to the liquid thermal conductivity, and $L = \mathbf{L}\mu^2/d^4g^2(\Delta\rho)^2$ is dimensionless latent heat. The first term in Eq. (21) is the energy required for evaporation, the second is the change of kinetic energy of the evaporating liquid molecules, the third is the net heat flux due to conduction, and the fourth is due to viscous dissipation.

The normal-stress condition is

$$E\Delta T_{SUP}^3 R(D_\rho - 1)J^2 + \hat{p} - p - h - \frac{2}{D_\rho(1 + h_x^2)}\left[(h_x^2 - 1)\hat{u}_x - h_x(\hat{u}_z + \hat{w}_x)\right] + \frac{2}{1 + h_x^2}\left[(h_x^2 - 1)u_x - h_x(u_z + w_x)\right] = \frac{h_{xx}}{B(1 + h_x^2)^{3/2}}, \quad (22)$$

where $B = d^2\Delta\rho g/\sigma$ is the ratio of gravity to surface tension force. If we consider the variation of surface tension due to temperature change, a thermocapillary parameter would appears in the left-side of Eq. (22), as in the work by Panzarella et al. [12]. The first term in Eq. (22) is due to vapor recoil (launching of the evaporating molecules with huge density jump across the interface), the forth term is due to hydrostatic pressure, and the term on the right-hand-side of the equation is due to capillary pressure.

The shear-stress boundary condition is

$$(1 - h_x^2)(u_z + w_x) - 4h_x u_x - D_\mu^{-1}[(1 - h_x^2)(\hat{u}_z + \hat{w}_x) - 4h_x\hat{u}_x] = 0, \quad (23)$$

and the continuity of tangential interfacial velocities requires

$$u - \hat{u} + h_x(w - \hat{w}) = 0. \quad (24)$$

The temperature across the evaporating interface is continuous

$$T = \widehat{T}, \quad (25)$$

and a linear relationship between the dimensionless temperature and the rate of evaporation is assumed to write

$$K\Delta T_{SUP}J = T, \quad (26)$$

where $K = k(8R_g T'^3_{SAT}\pi^{-1}m^{-3})^{1/2}/\mathrm{d}p'_{SAT}\mathbf{L}^2$ is the ratio of a typical evaporation rate for a film of thickness d to the absolute rate of evaporation at the saturation temperature. Here m is the moral mass of the vapor molecules, R_g is the ideal gas constant, and p'_{SAT} is the equilibrium vapor pressure at the temperature T'_{SAT}. A non-equilibrium evaporation equation for the interface, where both evaporation

and condensation occur, was derived by Schrage [14], and is linearized to Eq. (26), as discussed by Panzarella et al. [12]. Here $T = 0$ and $J = 0$ depicts an equilibrium state, $T > 0$ and $J > 0$ the evaporation, and $T < 0$ and $J < 0$ the condensation.

The conditions at the solid–vapor–liquid interface. called contact-line, are required. We assume that the vapor bubble is symmetric, and use the symmetry and the smoothness condition at $x = 0$ as

$$h_x = 0, \quad h_{xxx} = 0 \quad \text{at } x = 0. \tag{27}$$

The condition of contact, the condition of contact angle, and the constitutive equation between contact angle and contact-line are written as

$$h = 0, \quad h_x = \tan \Theta \quad \text{at } x = a(t), \tag{28}$$

$$\frac{\mathrm{d}a}{\mathrm{d}t} = E\Delta T_{\mathrm{SUP}} \frac{J(a)}{\sin \Theta} - \alpha(\Theta - \Theta_{\mathrm{c}}), \tag{29}$$

where α is a measurable quantity, and $J(a)$ is evaporative rate at the contact line.

Finally, the global mass balance is written as

$$\int_0^a (h_t - E \cdot \Delta T_{\mathrm{SUP}} \cdot J)\, \mathrm{d}x = 0, \tag{30}$$

which provides the kinematics of the interface in the presence of the mass flux across the interface.

3. Evolution equation

3.1. Lubrication approximation

We assume that $\epsilon = d/a_0$, the ratio of initial bubble thickness to its radius, is small, and apply the lubrication approximation. Details for the derivation of the evolution are given in the work by Panzarella et al. [12]. Interested readers may follow the analysis by noting that in the

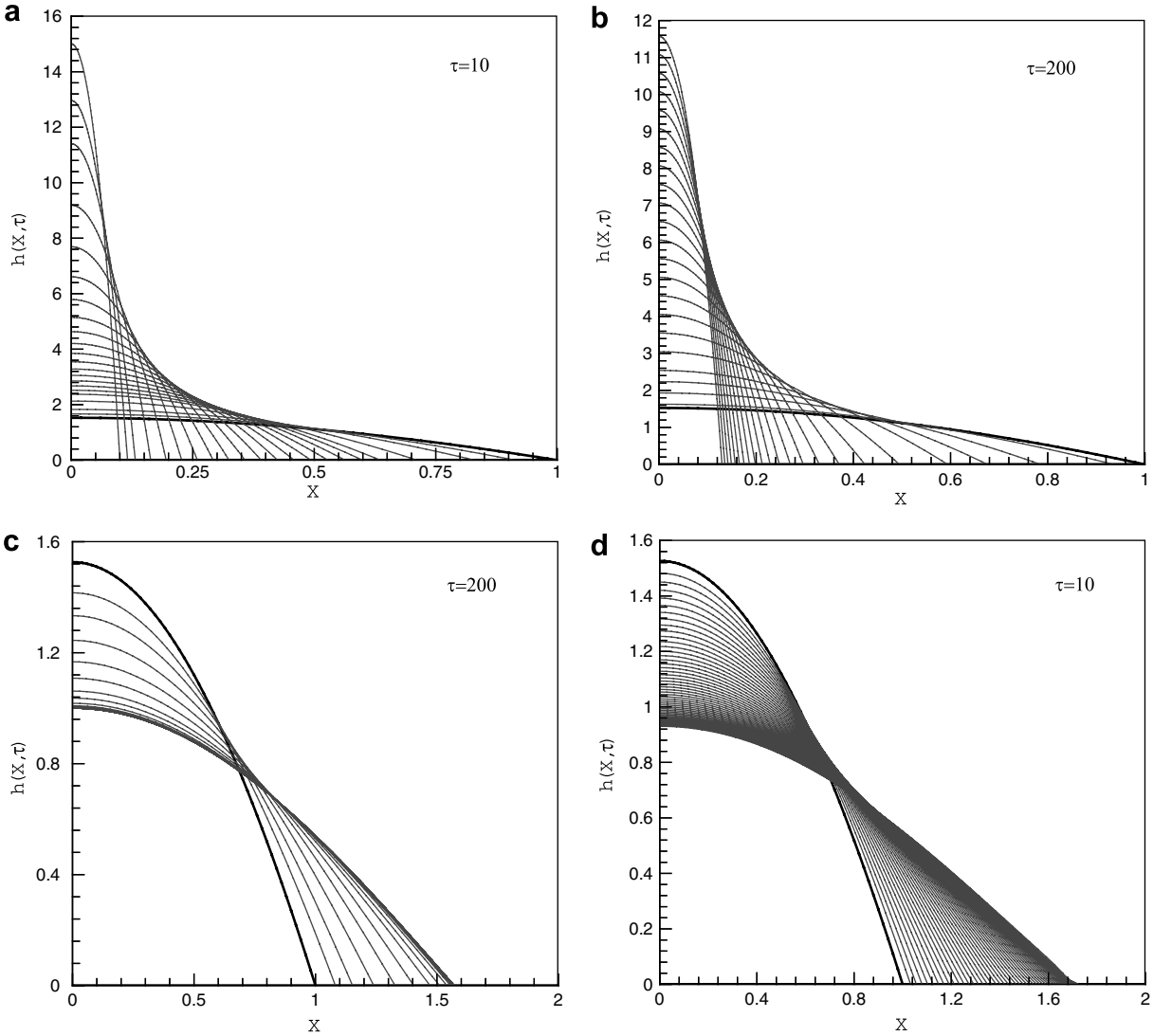

Fig. 3. Evolution of a bubble when $Q = 0$, $\overline{B} = 1$, $\underline{\beta} = 10^{-6}$ and $\underline{\alpha} = 0.1$. (a) $\Theta_{\mathrm{c}} = \pi/4$; (b) $\Theta_{\mathrm{c}} = \pi/2$; (c) $\Theta_{\mathrm{c}} = 3\pi/4$; (d) $\Theta_{\mathrm{c}} = 7\pi/8$.

present study we take $D_\mu = \epsilon \bar{D}_\mu$, which gives zero shear stress on the vapor–liquid interface.

New spatial and temporal variables are introduced as $X = \epsilon x$, $Z = \epsilon^{1/2} z$, $\zeta = \epsilon z$ and $\tau = \epsilon^3 t/3$, and all variables except the local bubble thickness h are expanded in power series for ϵ. The asymptotic expansions consistent with above assumption for vapor are

$$u(X,Z,\tau) = \epsilon u_0(X,Z,\tau) + \mathrm{O}(\epsilon^2), \tag{31}$$

$$w(X,Z,\tau) = \epsilon^2 w_0(X,Z,\tau) + \mathrm{O}(\epsilon^3), \tag{32}$$

$$p(X,Z,\tau) = p_0(X,Z,\tau) + \mathrm{O}(\epsilon), \tag{33}$$

$$T(X,Z,\tau) = \epsilon T_0(X,Z,\tau) + \mathrm{O}(\epsilon^2), \tag{34}$$

and those for liquid are

$$\hat{u}(X,\zeta,\tau) = \epsilon^2 \hat{u}_0(X,\zeta,\tau) + \mathrm{O}(\epsilon^3), \tag{35}$$

$$\hat{w}(X,\zeta,\tau) = \epsilon^2 \hat{w}_0(X,\zeta,\tau) + \mathrm{O}(\epsilon^3), \tag{36}$$

$$\hat{p}(X,\zeta,\tau) = \epsilon \hat{p}_0(X,\zeta,\tau) + \mathrm{O}(\epsilon^2). \tag{37}$$

The asymptotic expansions for the liquid and the solid temperature are

$$\widehat{T}(X,Z,\tau) = \epsilon \widehat{T}_0(X,Z,\tau) + \mathrm{O}(\epsilon^2), \tag{38}$$

$$\theta(X,Z,\tau) = \epsilon \theta_0(X,Z,\tau) + \mathrm{O}(\epsilon^2). \tag{39}$$

The asymptotic expansion for the mass flux is

$$J(X,\tau) = J_0(X,\tau) + \mathrm{O}(\epsilon), \tag{40}$$

and that for the contact angle is

$$\Phi(\tau) = \epsilon \Phi_0(\tau) + \mathrm{O}(\epsilon^2), (\Theta = \pi - \Phi). \tag{41}$$

3.2. Evolution equation

The governing equations and the boundary conditions can be solved sequentially by substituting the above expansions and reodering the terms in like order. Substituting some leading-order solutions into the mass-conservation

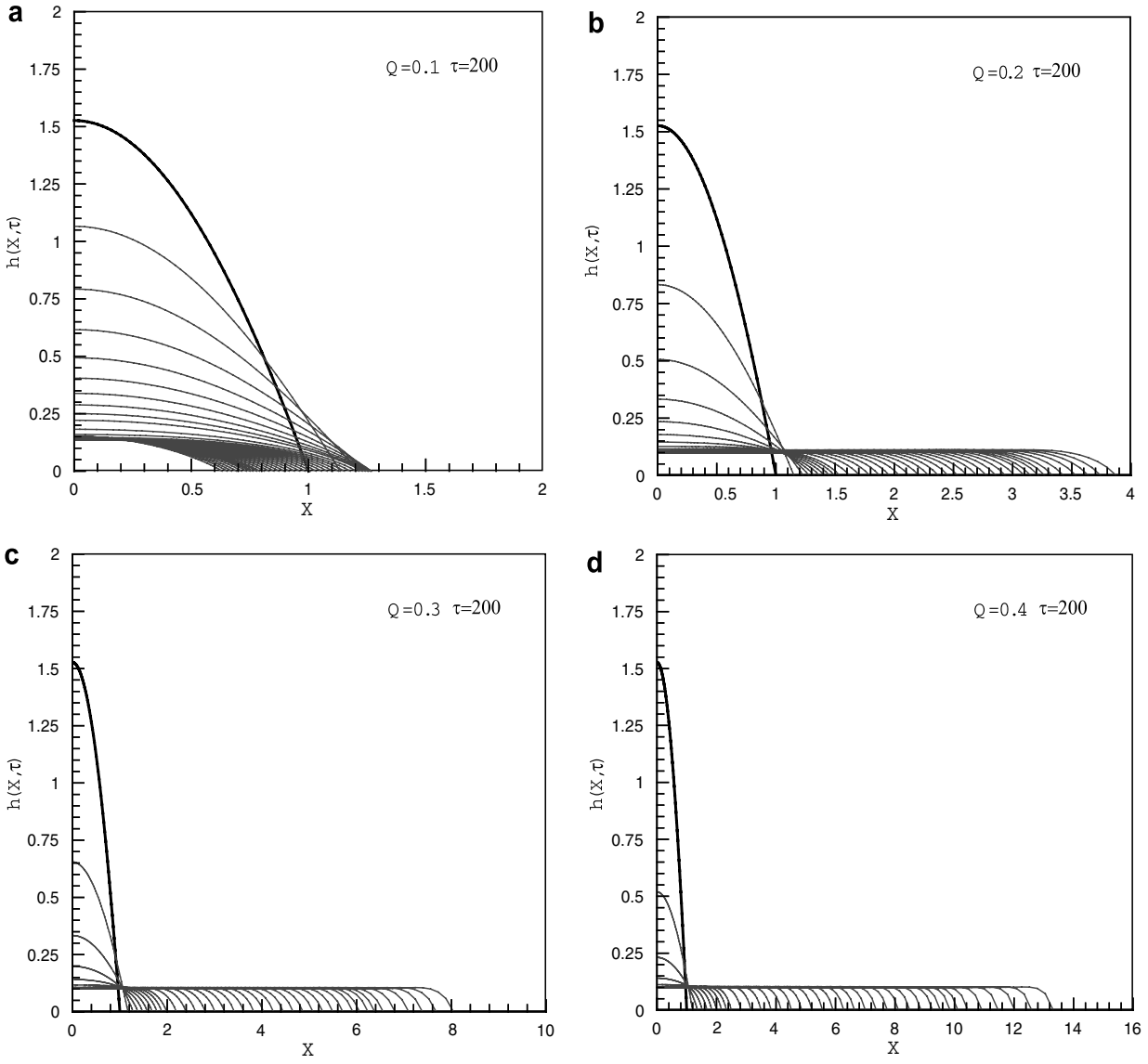

Fig. 4. Evolution of a bubble when $H = 0.1$, $\Theta_c = 3\pi/4$, $\overline{B} = 1$, $\underline{\beta} = 10^{-6}$, $\Lambda = 10$ and $\underline{\alpha} = 0.1$. (a) $Q = 0.1$; (b) $Q = 0.2$; (c) $Q = 0.3$; (d) $Q = 0.4$.

requirement results in a single, strongly-nonlinear evolution equation satisfied by the local vapor bubble thickness h,

$$h_\tau = Q\frac{1-h/H}{h+\Lambda} - \left[\left(h_X + \frac{1}{\overline{B}}h_{XXX}\right)(h^3+\underline{\beta}h)\right]_X. \tag{42}$$

The first term in the right-hand side of Eq. (42) represents evaporative mass loss, and the second term describes mass flux due to gravity and surface tension. The modified slip coefficient is so small ($\approx 10^{-6}$) that it can be taken as $\underline{\beta} = \beta$ and the Bond number is $\overline{B} = B/\epsilon^2$. This equation is almost identical to that derived by Panzarella et al. [12] except for the form of the slip-condition term. Q is now positive because the direction of evaporation is reversed from that of Burelbach and Bankoff [2], and the buoyancy term changes sign because the roles of liquid and vapor are interchanged. The surface tension term remains the same because a negative film curvature increases the local film pressure regardless of its phase. Thus, even though this equation resembles those used previously to study liquid film, the nature of its solutions can be quite different.

The parameter Q in Eq. (42) is

$$Q = \frac{3E\overline{B}(D_k z_L \Delta T_{SUP} - \Gamma_k z_S \Delta T_{SUB})}{B(K + D_k z_L)}, \tag{43}$$

which is directly proportional to subcooling or superheat, and measures the degree of heating from the solid plate. When $Q = 0$, the subcooling or superheat does not exist.

The parameter H in Eq. (42) is

$$H = D_k z_L \frac{\Delta T_{SUP}}{\Delta T_{SUB}} - \Gamma_k z_S, \tag{44}$$

which depends on the ratio of superheat and subcooling, and if $\Delta T_{SUB} \to \infty$, $H \to 0$. It thus measures the degree of subcooling.

The parameter Λ in Eq. (42) is

$$\Lambda = \frac{(\Gamma_k z_S + D_k z_L)K + D_k \Gamma_k z_L z_S}{K + D_k z_L}, \tag{45}$$

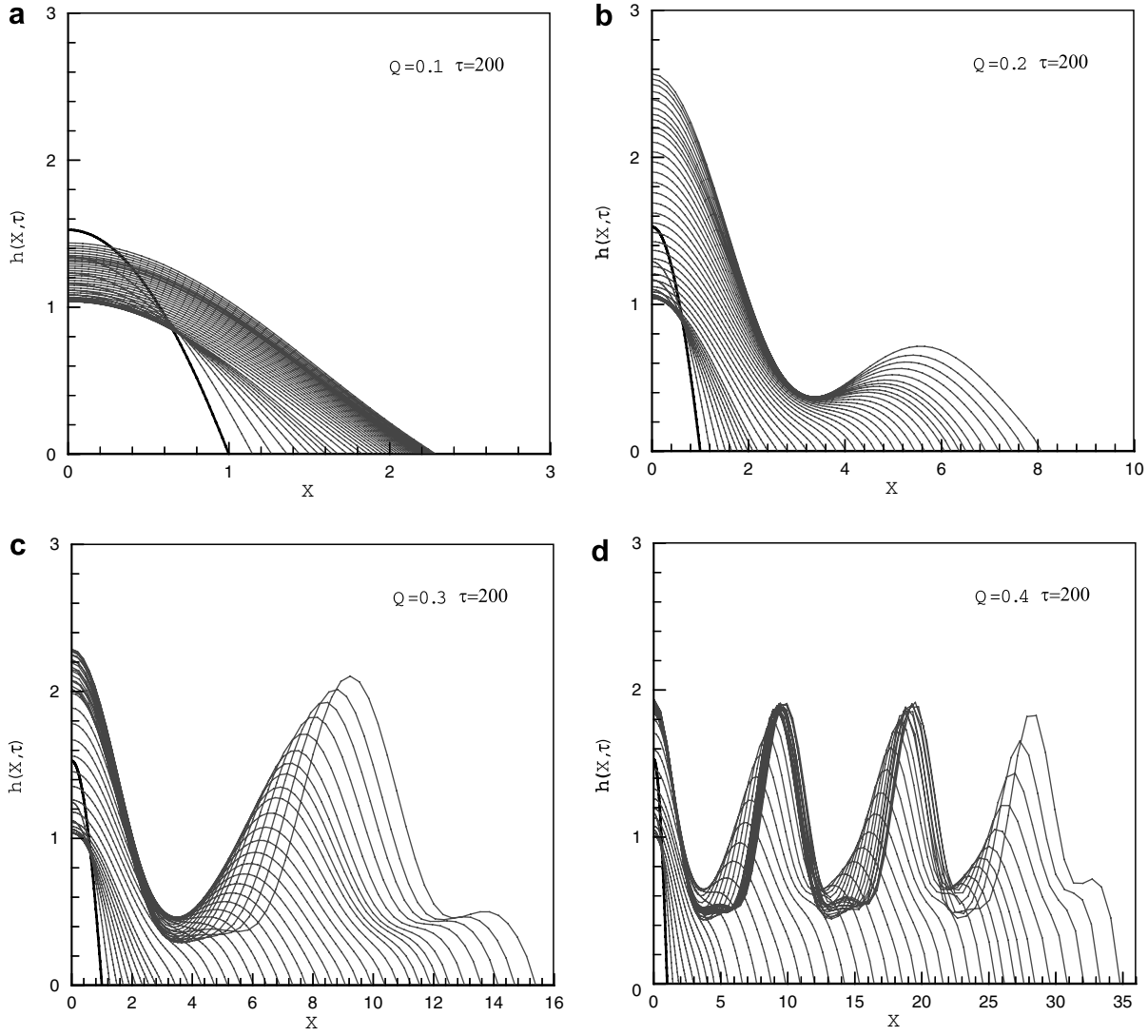

Fig. 5. Evolution of a bubble when $H = 1.0$, $\Theta_c = 3\pi/4$, $\overline{B} = 1$, $\underline{\beta} = 10^{-6}$, $\Lambda = 10$ and $\underline{\alpha} = 0.1$. (a) $Q = 0.1$; (b) $Q = 0.3$; (c) $Q = 0.5$; (d) $Q = 1.0$.

which accounts for the degree of non-equilibrium at the evaporating interface and the thermal resistance at the solid plate.

4. Numerical analysis

The evolution equation, a fourth-order nonlinear partial differential equation, is solved numerically with appropriate boundary conditions. The symmetry and smoothness condition at the center of the bubble are now

$$h_X = 0, \quad h_{XXX} = 0 \quad \text{at } X = 0, \tag{46}$$

and the contact condition and its angle at the contact-line $X = \bar{a}(\tau)$ become

$$h = 0, \quad h_X = \tan\Theta \quad \text{at } X = \bar{a}(\tau). \tag{47}$$

The location of the contact-line depends on the time, and the contact angle changes as the contact-line is moves. A constitutive equation for of $\bar{a}_\tau$ is thus required. As Anderson and Davis [1] explains, we write

$$\bar{a}_\tau = \frac{\mathbf{J_o}}{\sin\Theta} - \underline{\alpha}(\Theta - \Theta_c). \tag{48}$$

where $\bar{a} = \epsilon a$, $\mathbf{J_o} = Q/\Lambda$, $\underline{\alpha} = 3/\bar{\alpha}$, and Θ_c is the critical contact angle. The global mass balance [1]

$$\int_0^{\bar{a}} \left(h_\tau - Q\frac{1 - h/H}{h + \Lambda} \right) \mathrm{d}X = 0, \tag{49}$$

must also be invoked.

Initially the radius of vapor bubble is taken to be unity, and a quasi-steady state shape for h is assumed:

$$\bar{a}(0) = 1, \quad h(X,0) = \frac{\cos X - \cos(1)}{\sin(1) - \cos(1)}. \tag{50}$$

Eq. (50) describes a parabolic shape with an initial contact angle $\Theta_0 = 1.9144$.

Eq. (42) is a strongly nonlinear partial differential equation with the boundary conditions Eqs. (46)–(49) and the initial conditions Eq. (50). The lateral domain changes with time because the bubble front, or the contact-line location,

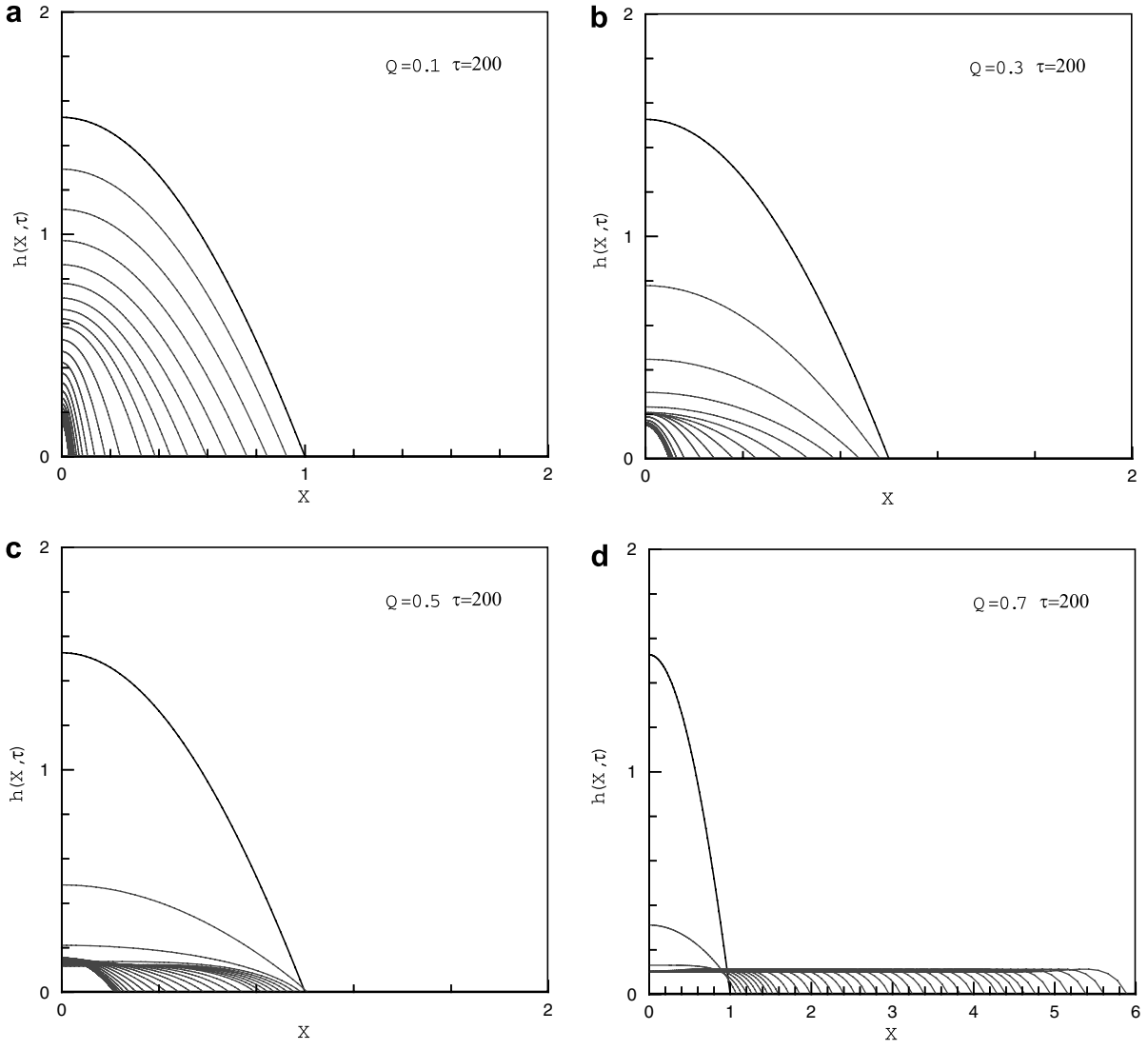

Fig. 6. Evolution of a bubble when $H = 0.1$, $\Theta_c = \pi/2$, $\overline{B} = 1$, $\underline{\beta} = 10^{-6}$, $\Lambda = 10$ and $\underline{\alpha} = 0.1$. (a) $Q = 0.1$; (b) $Q = 0.3$; (c) $Q = 0.5$; (d) $Q = 0.7$.

$X = a(\tau)$ depends on the time. The system is solved numerically using a finite-difference method. We begin by mapping the time-dependent computational domain into a fixed one with a change of variables

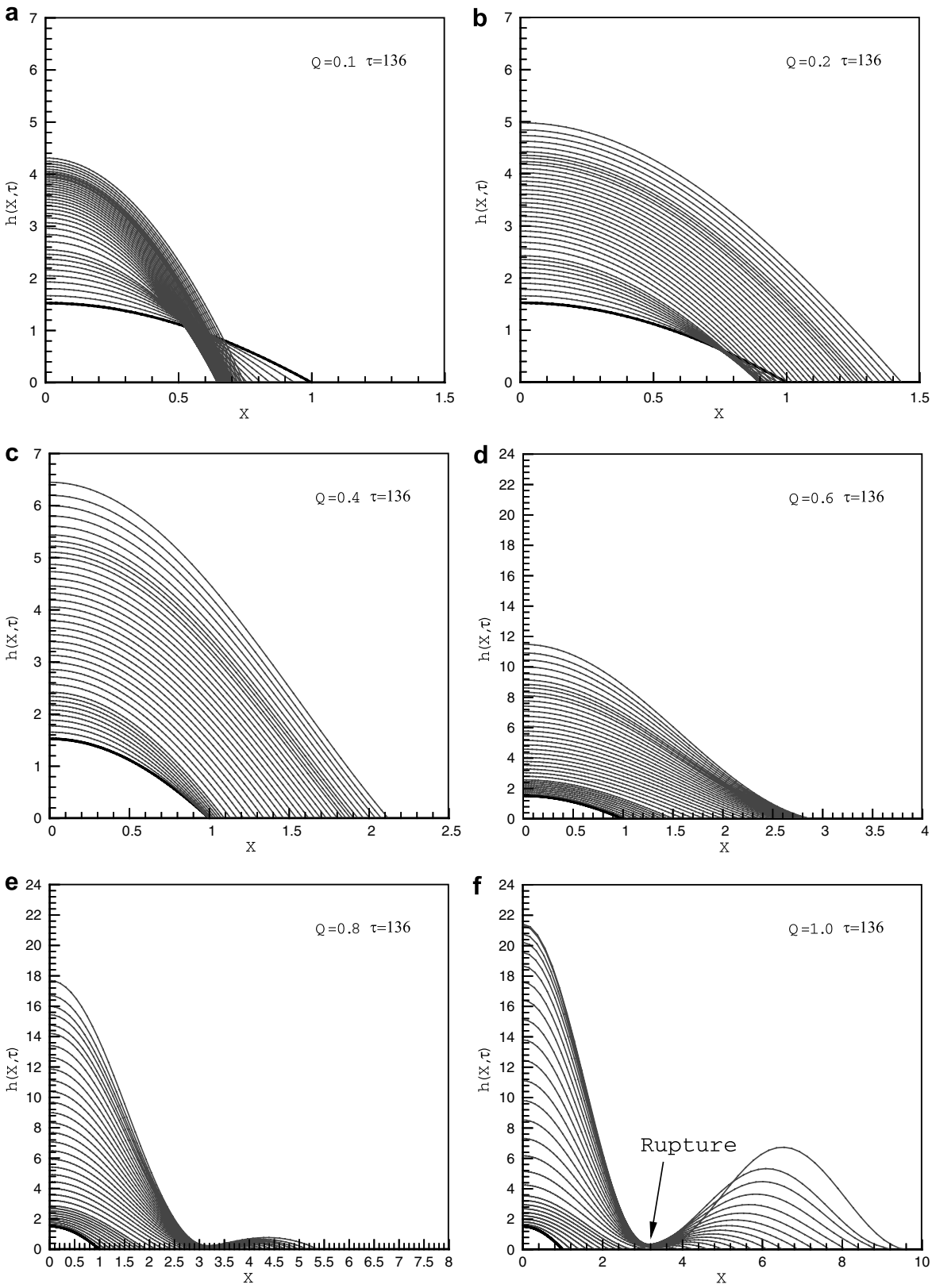

Fig. 7. Evolution of a bubble when $H = 100$, $\Theta_c = \pi/2$, $\overline{B} = 1$, $\underline{\beta} = 10^{-6}$, $\Lambda = 10$ and $\underline{\alpha} = 0.1$. (a) $Q = 0.1$; (b) $Q = 0.2$; (c) $Q = 0.4$; (d) $Q = 0.6$; (e) $Q = 0.8$; (f) $Q = 1.0$.

$$T = \tau, \quad \xi = \frac{1}{a(T)}X, \quad H(\xi,\tau) = h(X,T). \tag{51}$$

The computational domain is then given as $0 \leqslant \xi \leqslant 1$. Central difference in space is employed, while backward difference is used in time. The resulting difference equations are solved by the Newton–Raphson iteration.

5. Results and discussion

5.1. In case of $Q = 0$

When the superheat is absent ($Q = 0$), Eq. (42) is simplified as

$$h_\tau = -\left[\left(h_X + \frac{1}{\overline{B}}h_{XXX}\right)(h^3 + \underline{\beta}h)\right]_X. \tag{52}$$

We investigate the bubble behavior with $\overline{B} = 1$, $\underline{\alpha} = 0.1$, and $\underline{\beta} = 10^{-6}$, which are consistent with pure water. Fig. 3 shows the evolution of a bubble for four different values of Θ_c. When Θ_c is small as in Fig. 3a, the vapor–liquid interface near the contact line steepens with time to recover this small contact angle measured from the liquid side. As a result the width of the vapor bubble decreases. Although no volume change occurs in the vapor bubble, we classify this case as contraction of the vapor bubble. When the critical contact angle is increased to $\pi/2$, the rate of the bubble contraction is substantially decreased. In both cases the vapor–liquid interface steepens without bound, and the computation has to be terminated before the long-wave approximation used in deriving the evolution equation is violated. When the critical contact angle exceeds $\pi/2$, an equilibrium state is possible. Fig. 4c and d show such evolutions. In the cases shown the vapor bubble stays trapped between the liquid and the plate, and the Rayleigh–Taylor instability does not seem to break out for the disturbance wavelength contained.

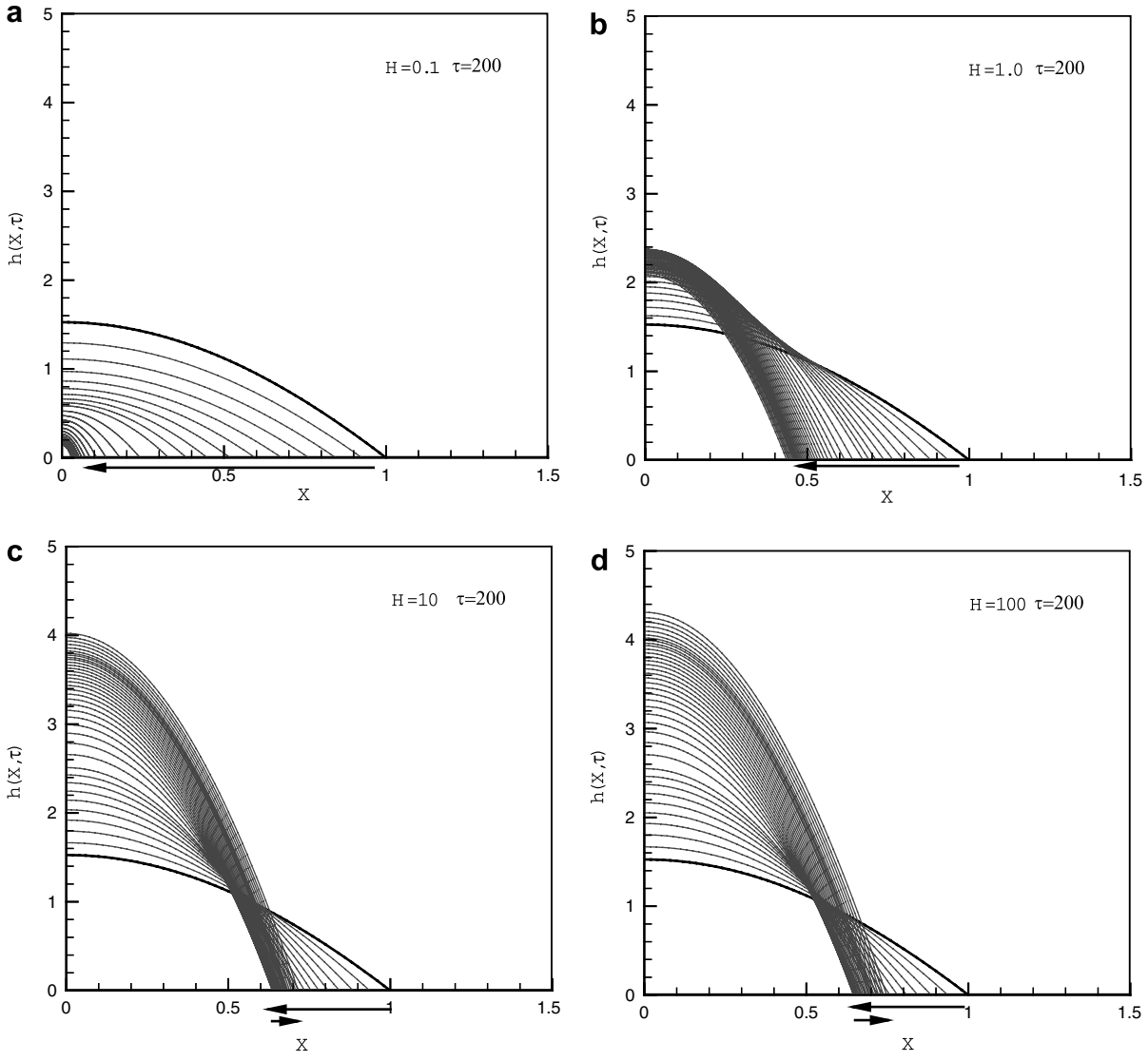

Fig. 8. Evolution of a bubble when $Q = 0.1$, $\Theta_c = \pi/2$, $\overline{B} = 1$, $\underline{\beta} = 10^{-6}$, $\Lambda = 10$ and $\underline{\alpha} = 0.1$. (a) $H = 0.1$; (b) $H = 1.0$; (c) $H = 10$; (d) $H = 100$.

5.2. In case of $Q \neq 0$

The bubble dynamics with evaporation ($Q \neq 0$) is shown in Figs. 4–8. We investigate the behavior of vapor bubble for four different value of $Q \geqslant 0.1$, $H \geqslant 0.1$, $0 \leqslant \Theta_c \leqslant \pi$ with $\Lambda = 10$, $\underline{\alpha}$ and $\underline{\beta} = 10^{-6}$, values consistent again with pure water. It is to be noted that the increase in the contact-line location $\bar{a}$ results in the expansion of vapor bubble and so the incipient recovery of the film boiling state. Its decrease on the other hand would indicate the evolution toward transition boiling. Through numerous computations of such cases we can construct an evolution map in a set of parameter space. In this study, we present evolution maps on the $1/Q$ vs. $1/H$ plane and the $1/Q$ vs. $1/\Theta_c$ plane.

5.2.1. 1/Q vs. 1/H plane

Fig. 4 shows the evolution of a vapor bubble for four different values of Q with $H = 0.1$, $\overline{B} = 1$, $\Lambda = 10$, $\underline{\beta} = 10^{-6}$, $\Theta_c = 3\pi/4$ and $\underline{\alpha} = 0.1$, which provides the high effect of subcooling ($H = 0.1$). When the degree of superheat is weak ($Q = 0.1$), the vapor bubble initially expands and then contracts, and the thickness of vapor bubble decreases to a constant value. When the degree of superheat is increased ($Q \geqslant 0.2$), the vapor bubble monotonously expands keeping a constant thickness. The moving front of the bubble is expected to merge with that from the neighboring bubble, and the film-boiling state will be reached. When the degree of superheat is further increased, the change in the thickness of the expanding bubble does not seem to be as drastic as that of the speed of the expanding front.

Fig. 5 shows the evolution of a vapor bubble for four different values of Q with $H = 1.0$, $\overline{B} = 1$, $\Lambda = 10$, $\underline{\beta} = 10^{-6}$, $\Theta_c = 3\pi/4$ and $\underline{\alpha} = 0.1$, which provides an example of moderate subcooling ($H = 1.0$). The vapor bubble eventually expands for all values of Q chosen. However, significant corrugations appear on the vapor–liquid interface as Q is increased. As seen in Fig. 5d, the evolution toward film boiling occurs with a large-amplitude wave motion on the vapor–liquid interface. It is interesting to note that the interfacial instability of the vapor–liquid interface shown bears the possibility of interface rupture for even weaker subcooling (higher H).

Fig. 6 shows the evolution of a vapor bubble for four different values of Q with $H = 0.1$, $\overline{B} = 1$, $\Lambda = 10$, $\underline{\beta} = 10^{-6}$, $\Theta_c = \pi/2$ and $\underline{\alpha} = 0.1$, which provides the strong effect of subcooling ($H = 0.1$) and a different critical angle ($\Theta_c = \pi/2$). The vapor bubble contracts and reaches an equilibrium state with constant h and $\bar{a}$ for $\Theta_c < 0.7$. When $\Theta_c > 0.7$ the vapor bubble appears to expand and reaches an equilibrium state with constant film thickness, which shows recovery to the film boiling. There are contraction or expansion of the vapor bubble depending on the value of Q. The degree of the contraction appears somewhat similar to each other, while the degree of the expansion appears to increase as Q increases.

Fig. 7 shows the evolution of a vapor bubble for the six different values of Q with $H = 100$, $\overline{B} = 1$, $\Lambda = 10$, $\underline{\beta} = 10^{-6}$, $\Theta_c = \pi/2$ and $\underline{\alpha} = 0.1$, which provides the high effect of superheat ($H = 100$). Since the effect of superheat is much stronger than the effect of the subcooling, the dynamics of vapor bubble appears different from that shown in Fig. 6. When Q is small, the vapor bubble contracts and then expands, where the range of contraction is wider than the range of expansion. As Q increases, the contraction and expansion of vapor bubble also appears. However the range of contraction becomes small and disappears. When Q is much larger, the vapor bubble doses not expand with constant thickness, but vapor–liquid interface becomes corrugated with a possibility of rupture for high enough Q.

Fig. 8 shows the evolution of a vapor bubble for four different values of H with $Q = 0.1$, $\overline{B} = 1$, $\Lambda = 10$, $\underline{\beta} = 10^{-6}$, $\Theta_c = \pi/2$ and $\underline{\alpha} = 0.1$. When H is small, the vapor bubble monotonously contracts until it reaches an equilibrium. The effect of subcooling makes the vapor bubble to contract until the vapor–liquid interface gets close enough to the solid plate, where an equilibrium between these two effects is reached. As H is increased, the range of contraction becomes small, and the equilibrated vapor bubble grows in size. With much weaker subcooling, the initial contraction of the bubble can be followed by subsequent expansion.

Fig. 9 shows an evolution map on the $1/Q$ vs. $1/H$ plane for three different values of critical angle Θ_c. Four different evolutions of the vapor bubble are indicated, which are monotonous contraction, contraction–expansion, expansion–contraction, and monotonous expansion. In case of $\Theta_c = 3\pi/4$, the eventual contraction occurs for small

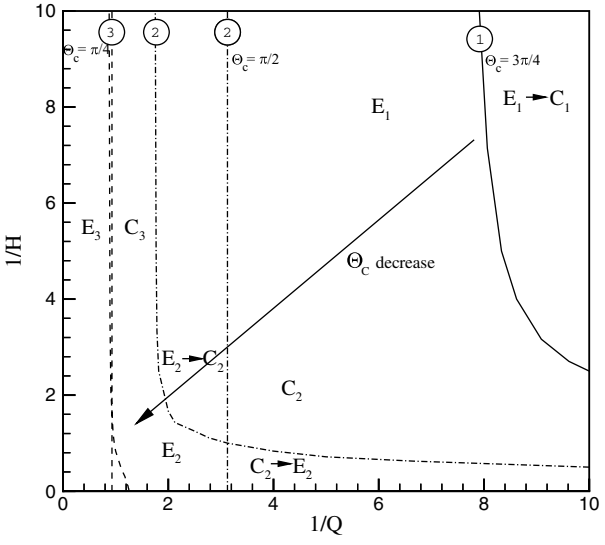

Fig. 9. $1/Q$ vs. $1/H$ plane for the case $\Theta_c = \pi/4$, $\Theta_c = 2\pi/4$ and $\Theta_c = 3\pi/4$. E: expanding region of the vapor bubble, C: contraction region of the vapor bubble, $C \rightarrow E$: expanding region of the vapor bubble after contracting initially, $E \rightarrow C$: contacting region of the vapor bubble after expanding initially. Line (1) for $\Theta_c = 3\pi/4$, Line (2) for $\Theta_c = 2\pi/4$ and Line (3) for $\Theta_c = \pi/4$.

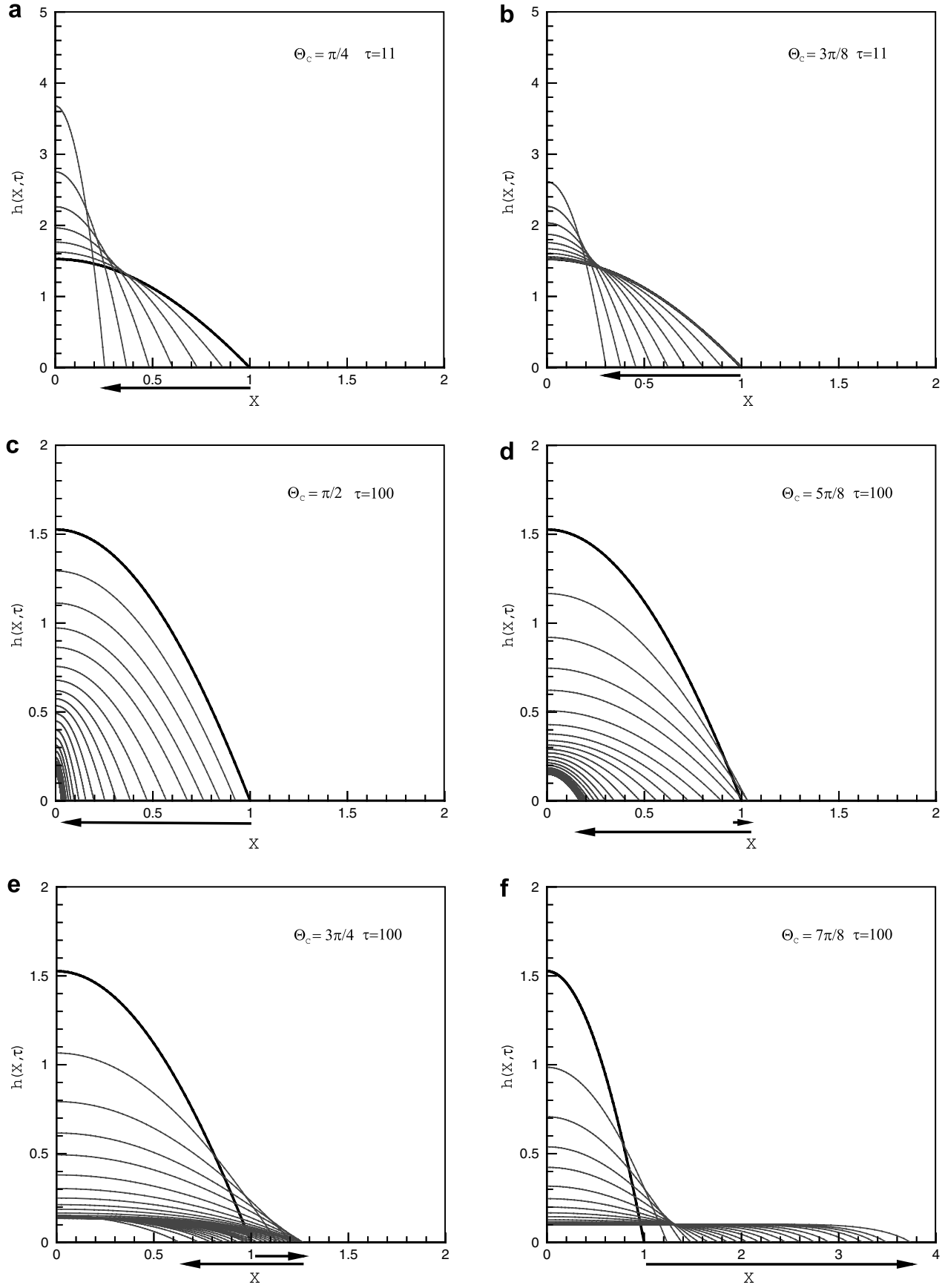

Fig. 10. Evolution of a bubble when $Q = 0.1$, $H = 0.1$, $\overline{B} = 1$, $\underline{\beta} = 10^{-6}$, $\Lambda = 10$ and $\underline{\alpha} = 0.1$. (a) $\Theta_c = \pi/4$; (b) $\Theta_c = 3\pi/8$; (c) $\Theta_c = \pi/2$; (d) $\Theta_c = 5\pi/8$; (e) $\Theta_c = 3\pi/4$; (f) $\Theta_c = 7\pi/8$.

enough Q and large enough H. The region for the expansion (film boiling) thus is for strong enough superheat and weak enough subcooling. When $\Theta_c = \pi/2$ all four different behaviors are clearly seen. The map shows the boundaries for these different evolutions, and can be used in predicting the transition and film boiling. When $\Theta_c = \pi/4$ the region of contraction dominates in the range shown in Fig. 9. The regions for contraction–expansion and expansion–contraction are barely seen in the scale used. The upper region in-between Line (3) is for expansion–contraction, while the lower region between Line (3) is for contraction–expansion. It is also noted that the region for contraction becomes increases, and so that for expansion decreases, as the critical contact angle is decreased, which suggests that the recovery to the film boiling state is more likely with a larger critical angle (less wetting surface).

5.2.2. $1/Q$ vs. Θ_c plane

Fig. 10 shows the evolution of a vapor bubble for six different values of Θ_c with $Q = 0.1$, $H = 0.1$, $\overline{B} = 1$, $\Lambda = 10$, $\underline{\beta} = 10^{-6}$ and $\underline{\alpha} = 0.1$. The effects of subcooling and superheat are comparable. When the critical contact angle is small, the vapor bubble contracts, and its thickness increases. When the critical angle is between $\pi/2$ and $5\pi/8$, the vapor bubble contracts, and its thickness decreases. However, an expansion of the vapor bubble occurs in Fig. 10d. When the critical angle is even higher, the range of expansion increases, while the range of contraction decreases. The vapor bubble eventually expands with constant thickness, as shown in Fig. 10e.

Fig. 11 shows another evolution map for the vapor bubble. Four different evolutions are predicted on the $1/Q$ vs. Θ_c plane for different values of H, $Q > 0.1$, and

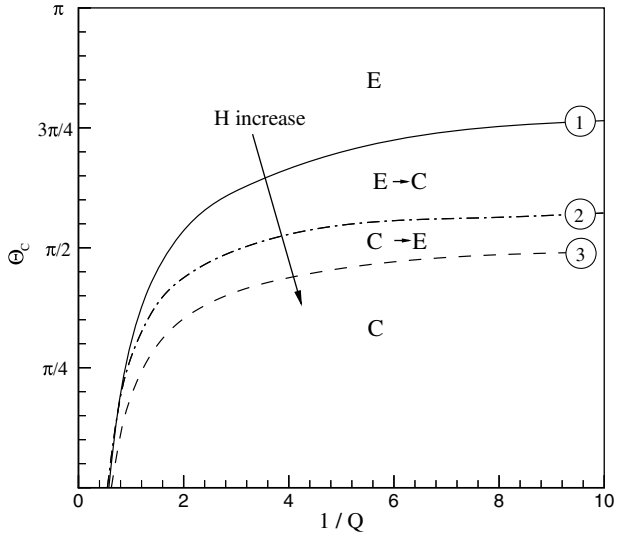

Fig. 11. $1/Q$ vs. Θ_c plane for evolution of $\bar{\alpha}$, E: expanding region of the vapor bubble, C: contracting region of the vapor bubble, $C \to E$: expanding region of the vapor bubble after contracting initially, $E \to C$: contacting region of the vapor bubble after expanding initially. Line (1) for $H = 0.1$, Line (2) for $H = 0.1, 1, 10, 100$ and Line (3) for $H = 10, 100$.

$0 \leqslant \Theta_c \leqslant \pi$. As H increases, which means the weaker subcooling effect, the region of expansion of vapor bubble grows, the region of expansion–contraction appears to disappear, and the region of contraction–expansion emerges. In the region of vapor bubble expansion the rate of $\bar{a}$ increase grows, as the critical angel increases, while in the region of vapor bubble contraction the rate of $\bar{a}$ decrease grows, as the critical angel decreases.

6. Conclusions

A two-dimensional vapor bubble due to liquid evaporation on a heated solid plate is studied with a focus on the dynamics of its interface with the vapor phase. the dynamics of bubble is mainly induced by the superheat from the solid plate, the subcooling from liquid above, and wettability of the liquid on the solid plate.

The dynamics of the vapor bubble is investigated by deriving an evolution equation based on the lubrication theory and a subsequent numerical analysis. Five different behaviors of vapor bubble are obtained from Eq. (42): (1) the monotonous expansion of bubble shown in Fig. 4; (2) the monotonous contraction of bubble shown in Fig. 6a–c; (3) the contraction–expansion of bubble shown in Fig. 8c, d; (4) the expansion–contraction of bubble shown in Fig. 9d, e, and (5) the contraction–equilibrium of bubble shown in Fig. 6a. Moreover, with the parameter H, accounting for the degree of superheat from the solid plate, the parameter Q, accounting for the degree of supercooling through liquid, and the parameter Θ_c, accounting for the dewetting/wetting characteristics of liquid on the solid plate, we present maps for these different evolutions on the $1/Q$ vs. $1/H$ plane and the $1/Q$ vs. Θ_c plane, which can be a useful guide in the study of the film and the transition boiling.

Acknowledgements

The authors thank Professor Stephen H. Davis and George Bankoff for their guidance with the formulation of the present problem and Jinhong Park for his contribution to the initial stages of the numerical analysis. This work is supported by the National Center for Nanomaterials Technology of Pohang, Korea.

References

[1] D.M. Anderson, S.H. Davis, The spreading of volatile liquid droplets on heated surfaces, Phys. Fluids 7 (2) (1995) 248–265.
[2] J.P. Burelbach, S.G. Bankoff, Nonlinear stability of evaporating/condensing liquid films, J. Fluid Mech. 195 (1988) 463–494.
[3] Van P. Carey, Liquid phase-change phenomena, Hemisphere, New York, 1992.
[4] J.M. Delhaye, Jump conditions and entropy sources in two-phase systems, Int. J. Multiphase Flow 1 (1974) 395–409.
[5] V.K. Dhir, Boiling heat transfer, Annu. Rev. Fluid Mech. 30 (1998) 365–401.
[6] S.H. Davis, Contact-line problems in fluid mechanics, J. Fluid Mech. 50 (1983) 977–982.

[7] V. Dussan, S.H. Davis, On the motion of a fluid–fluid interface along a solid surface, J. Fluid Mech. 65 (1974) 71–95.
[8] V. Dussan et al., On the spreading of liquids on solid surface: static and dynamic contact lines, Annu. Rev. Fluid. Mech. 11 (1979) 371–400.
[9] P. Ehrhard, S.H. Davis, Non-isothermal spreading of liquid drops on horizontal plates, J. Fluid Mech. 229 (1991) 365–388.
[10] J.P. Haley, M.J. Miksis, The effect of the contact line on droplet spreading, J. Fluid Mech. 223 (1991) 57–81.
[11] A. Oron, S.H. Davis, Long-scale evolution of thin liquid films, Rev. Mod. Phys. 69 (3) (1997) 931–979.
[12] C.H. Panzarella, S.H. Davis, S.G. Bankoff, Nonlinear dynamics in horizontal film boiling, J. Fluid Mech. 402 (2000) 163–194.
[13] W.M. Rohsenow, Boiling. Annu. Rev. Fluid Mech. 3 (1971) 211–236.
[14] R.W. Schrage, A theoretical study of interphase mass transfer, Columbia University Press, New York, 1953.
[15] L.C. Witte, J.H. Lienhard, On the existence of two transition boiling curves, Int. J. Heat Mass Transfer 25 (1982) 771–779.